RAPID COMMUNICATIONS

PHYSICAL REVIEW B VOLUME 48, NUMBER 4 15 JULY 1993-II

Observation of higher-order Raman modes in C_{60} films

Zheng-Hong Dong, Ping Zhou, J.M. Holden, and P.C. Eklund
Department of Physics and Astronomy, University of Kentucky, Lexington, Kentucky 40506

M. S. Dresselhaus
Department of Electrical Engineering and Computer Science and Department of Physics, Massachusetts Institute of Technology, Cambridge, Massachusetts 02139

G. Dresselhaus
Francis Bitter National Magnet Laboratory, Massachusetts Institute of Technology, Cambridge, Massachusetts 02139
(Received 7 April 1993)

Raman spectra for oxygen-free solid C_{60} films were obtained at $T = 20$ and 523 K. Using higher laser intensity at temperatures where photopolymerization is not important, over 100 Raman lines were observed and assigned to combination and overtone scattering from intramolecular vibrational modes and to otherwise Raman-inactive modes activated by isotopic substitution ($^{13}C^{12}C_{59}$). Values for nearly all of the silent mode frequencies are thereby obtained.

The Raman spectrum of C_{60} is unique relative to other materials insofar as the first-order spectrum in the solid state is almost identical to that of the free molecule, thereby providing strong evidence for the almost ideal molecular nature of solid C_{60}.[1] Specifically, the $T = 300$ K spectrum shows 12 strong features, ten of which are identified with the Raman-allowed A_g (2 modes) and H_g (8 modes) vibrations.[1] When Raman spectra are taken below the orientational ordering temperature $T_0 \sim 260$ K of C_{60}, or above the thermal decomposition temperature $T_p \sim 450$ K for the photopolymer,[2,3] it is possible to expose the C_{60} films to sufficiently high laser excitation intensities to study numerous weaker features in the Raman spectrum in detail, without polymerizing or inflicting photoinduced damage to these films.[2–4]

In this paper, we report Raman spectra over the range 150–3500 cm^{-1} associated with numerous combination and overtone modes of the fundamental vibrational modes of C_{60}. The higher-order spectra observed here are unusual for a solid, both in terms of the richness of the spectra, and the sharpness of the spectral features, consistent with the molecular nature of solid C_{60}. Group-theoretical arguments are presented to specify the various mode symmetries that can be observed in a second-order intramolecular Raman-scattering process.

Values for almost all of the intramolecular vibrational modes are available from Raman, IR, electron-energy-loss spectroscopy, luminescence, and neutron-scattering measurements.[5] Of these various methods, Raman and IR spectroscopies are expected to give the most accurate values for the mode frequencies because of their higher intrinsic resolution. Thus the second-order Raman spectrum provides an opportunity to determine more accurately the mode frequencies and symmetries of some of the "silent modes." Silent modes can also be activated by isotopic substitution (i.e., $^{13}C^{12}C_{59}$), as was previously reported, e.g., in benzene.[6]

The present work is also significant for providing further evidence for the molecular nature of solid C_{60}, for expanding the possibilities of the experimental observation and identification of silent modes in C_{60}, and for pointing to an experimental approach that yields a detailed examination of fine structure in the Raman spectrum. Because of the molecular nature of C_{60} and the high symmetry of the isolated C_{60} molecule, C_{60} appears to be a prototype molecular solid for detailed spectroscopic studies which were previously possible only in the gas phase, or in solution.

Raman spectra at temperatures $T = 20$ and 523 K for solid C_{60} films (~7000 Å) are shown in Fig. 1. From group-theoretical considerations,[7] the expected number of second-order Raman lines ($\omega_1 + \omega_2$) is very large, consisting of a total of 151 modes with A_g symmetry, and 661 modes with H_g symmetry.

We find experimentally that many of the strongest second-order Raman lines involve only modes which are also observed in first order. This general subset of overtones and combination modes is calculated by taking the direct product $(2A_g + 8H_g) \otimes (2A_g + 8H_g)$, and taking care not to double count. These special second-order modes have been marked on Fig. 1 and account well for most of the intense second-order Raman features above ~1000 cm^{-1} (see Table I). Somewhat weaker features in the Raman spectra might be expected to arise from combination modes where only one of the components relates to first-order Raman-active lines. In this case, combination modes with A_g or H_g symmetry arise from the direct product $(2A_g + 8H_g) \otimes \Gamma_f$, where the vibrational modes with Γ_f symmetry are not active in the first-order Raman spectrum. In this category, there are no modes in the direct product with A_g symmetry, and 156 modes with H_g symmetry, in the second-order spectrum. Yet weaker lines in the second-order Raman spectra could arise from either overtones or combination modes of the same parity, through the direct product $\Gamma_i \otimes \Gamma_f$, where Γ_i and Γ_f are both identified with Raman-inactive modes.

A variety of experimental techniques shows that an orientational order-disorder transition occurs in solid C_{60}

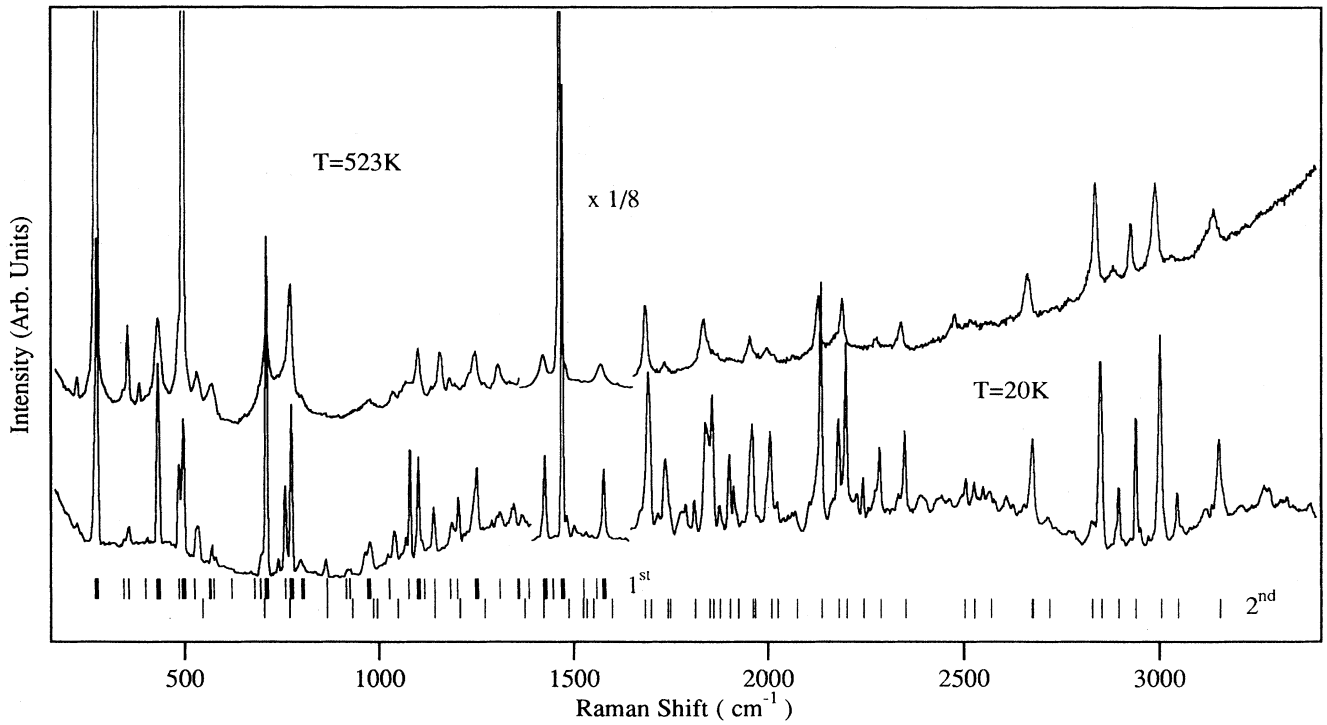

FIG. 1. Raman spectra for solid C_{60} films (~7000 Å thick) taken at temperatures $T = 523$ K and 20 K using 488.0-nm Ar laser radiation. The mode frequencies shown schematically in the figure are as follows: (upper, marked first) gives the position of all 46 fundamental frequencies and the Raman-allowed modes are marked as darker ticks, and (lower, marked second) gives the position of all overtone and combination modes $(\omega_1 + \omega_2)$ derived from the dot product $(A_g + H_g) \otimes (A_g + H_g)$ (see Table I). Details regarding the film preparation and spectroscopy are found in Ref. 1.

at $T_0 \sim 260$ K.[8,9] Below T_0 and above $T_p \sim 450$ K photopolymerization does not seem to occur.[2] Above T_p the fullerene balls are spinning rapidly about their fcc lattice positions and any photoinduced dimers C_{60}=C_{60} that might be formed by the Raman laser will be thermally decomposed.[2] Thus solid C_{60} at $T = 523$ K provides an opportunity to study the intramolecular modes both with crystal-field splittings removed from consideration by inhomogeneous broadening, and with thermal decomposition of dimers offsetting the photopolymerization effect. As C_{60} is cooled below T_0, the balls first adopt an orientational ratcheting motion about any of four distinct (111) axes, and this motion is gradually frozen out, as the material is cooled to low T. A merohedrally disordered solid phase[8,9] is found at 20 K where the low T Raman spectrum was taken. Crystal-field-induced splittings of the first-order Raman H_g symmetry intramolecular modes are expected at these low temperatures. However, the size of the splittings, and the extent of the Raman activity of the new Raman lines, cannot be predicted by group theory. While crystal-field splittings were reported previously,[10] these authors did not consider the possibility of second-order Raman processes or isotopically activated silent modes (e.g., $^{13}C^{12}C_{59}$).

The possibility of observing Raman-forbidden modes due to symmetry lowering associated with isotopic enrichment has been reported previously for benzene.[6] The natural abundance of ^{13}C is about 1.1% which implies that there is a 66% probability that a fullerene molecule is $^{13}C^{12}C_{59}$ rather than $^{12}C_{60}$. Thus in our films one would expect roughly equal amounts of $^{13}C^{12}C_{59}$ and $^{12}C_{60}$. The presence of a single ^{13}C atom in a fullerene molecule has two effects. First, the Raman-active modes should soften slightly, as the dynamic mass in the eigenmodes is diminished slightly by the isotopic substitution. Second, the icosahedral symmetry is broken which leads to the Raman activation and the splitting of all possible modes and to the splitting of degenerate modes. Below ~1500 cm^{-1} we find several Raman lines which can be assigned to these broken-symmetry modes.

We first consider the low- and high-T spectra of Fig. 1 in the region below the highest frequency first-order Raman mode $H_g(8) = 1577.5$ cm^{-1}. In Fig. 1 (below the spectra) we indicate the ten first-order Raman modes $(2A_g + 8H_g)$ by a thick vertical bar to aid in their identification relative to other intraball vibrational modes. These lines are generally much more intense than the other features in Fig. 1. Since crystal-field-induced splittings are not possible at these temperatures, it is natural to assign the additional (~ 20) lines observed below ~1700 cm^{-1} to second-order scattering involving intramolecular modes (where $\omega_1 \pm \omega_2$ are the frequencies for symmetry-allowed, gerade pairs). If solid-state effects produce phonon band dispersion, then $\omega_1(q)$ and $\omega_2(-q)$ represent the pairings, and structure in the second-order Raman spectrum is expected at frequencies corresponding to maxima in the density of states, i.e., either at $q = 0$ or at the Brillouin-zone edges. Consistent with the ob-

servation of sharp second-order lines, we make here the simplest assumption that only $q = 0$ modes participate. With these constraints, the lowest allowed sum mode is $2H_g(1)$ with frequency 546 cm^{-1}. There are eight observed lines with frequencies less than 546 cm^{-1}, three of which are first-order allowed (see Table I). The remaining five modes cannot be assigned to difference mode scattering [i.e., $\omega_1(\Gamma_i) - \omega_2(\Gamma_f)$] and are assigned to isotopically activated modes. Above 546 cm^{-1}, an additional ~14–20 sharp lines can be detected which are assigned to second-order $(\omega_1 + \omega_2)$ scattering. Possible assignments to isotopically activated modes are also given in Table I.

The first-order lines in the high-T spectrum appear to have their counterparts in the low-T spectrum, since small temperature-dependent frequency shifts (~5 cm^{-1}) are difficult to observe on the scale of Fig. 1. More importantly, almost every feature in the high-T spectrum below ~1700 cm^{-1} appears in the low-T spectrum, albeit with reduced linewidth. Therefore, since we cannot attribute any of the high-T lines to crystal-field effects, we must assign these same features to either second-order scattering or to isotopically activated modes in the previously discussed low-T crystalline phase of C_{60}.

TABLE I. Observed and assigned Raman lines in cm^{-1} in C_{60} taken on films at 20 K and single crystals at 40 K.

Identification[a]	[n][b]	Model	20 K	40 K[c]
$H_g(1)$		273.0[d]	273.0	272
$H_g(3) - H_g(2)$		278.5		
$H_g(7) - H_g(5)$		325.5		
$H_g(5) - H_g(4)$		326.0		
$H_g(4) - H_g(2)$		342.5	343.5	
$H_u(1)$[e]		342.5	343.5	
$F_{2u}(1)$[e]		355.5	355.5	
$G_u(1)$[e]		399.5	404.5	
$H_g(2)$		432.5[d]	432.5	433
$H_g(8) - H_g(5)$		476.5		
$G_g(1)$[e]		486.0	486.5	485
$A_g(1)$		497.5[d]	497.5	496
$F_{1u}(1)$[e]		526.5	533.5	533
$2H_g(1)$		546.0		
$F_{2g}(1)$[e]		566.5	570.0	567
$F_{1u}(2)$[e]		575.8	580.5	
$H_g(5) - H_g(2)$		668.5		
$2H_u(1)$		685.0		
$F_{2u}(1) + H_u(1)$[f]		698.0	692.0	696
$H_g(1) + H_g(2)$		705.5		
$H_g(3)$		711.0[d]	711.0	709
$2F_{2u}(1)$		711.0		
$G_u(1) + H_u(1)$		742.0	742.0	738
$F_{2u}(1) + G_u(1)$		755.0	758.5	757
$G_g(1) + H_g(1)$[f]		759.0	758.5	757
$A_g(1) + H_g(1)$		770.5		
$F_{1g}(1) + H_g(1)$		775.0	775.0	772
$H_g(4)$		775.0[d]	775.0	772
$2G_u(1)$[f]		799.0	798.5	796
$H_g(5) - H_g(1)$		828.0		
$F_{2g}(1) + H_g(1)$		839.5		
$2H_g(2)$[f]		865.0	862.5	860
$F_{1u}(2) + H_u(1)$		918.3		914
$G_g(1) + H_g(2)$[f]	1	918.5	919.5	922
$A_g(1) + H_g(2)$		930.0		
$G_u(1) + H_u(2)$		962.5	962.5	959
$2G_g(1)$		972.0	976.0	972
$A_g(2) - A_g(1)$[f]		972.5	976.0	972
$F_{1u}(2) + G_u(1)$		975.3	976.0	972
$H_g(1) + H_g(3)$		984.0		
$2A_g(1)$		995.0		
$2F_{1g}(1)$		1004.0		
$F_{2u}(2) + H_u(1)$[f]		1022.5	1022.5	1022
$H_u(1) + H_u(3)$[f]		1038.5	1040.0	1038
$H_g(1) + H_g(4)$		1048.0		
$2F_{1u}(1)$		1053.0		
$F_{1g}(1) + F_{2g}(1)$		1068.5	1068.5	1079
$G_g(3) + H_g(1)$[f]	1	1079.0	1080.0	1079
$H_g(5)$		1101.0[d]	1101.0	1099
$F_{1u}(1) + F_{1u}(2)$	1	1102.3	1101.0	1099
$H_g(2) + H_g(3)$[f]	3	1143.5	1141.0	1138
$F_{1u}(3)$[e]		1182.9	1187.0	
$F_{2g}(3) + H_g(1)$	1	1187.0	1187.0	
$H_g(2) + H_g(4)$[f]		1207.5	1204.0	1200
$A_g(1) + H_g(3)$		1208.5	1204.0	1200
$H_g(6)$		1251.0[d]	1251.0	1252
$A_g(1) + H_g(4)$		1272.5		
$G_g(1) + G_g(3)$	1	1292.0	1289	
$G_u(4) + H_u(1)$[f]	1	1312.5	1310.5	
$F_{2g}(3) + H_g(2)$	1	1346.5	1346.0	1345
$H_g(1) + H_g(5)$	2	1374.0	1368.0	
$F_{1g}(2) + H_g(2)$		1408.0	1410.0	1406
$F_{1g}(1) + F_{2g}(3)$		1416.0		1417
$2H_g(3)$		1422.0		
$H_g(7)$		1426.5[d]	1426.5	1425
$F_{1u}(1) + G_u(3)$[f]		1450.5	1450.5	
$A_g(2)$		1470.0[d]	1470.0	1468
$H_g(3) + H_g(4)$	2	1486.0	1481.0	1480
$F_{1u}(2) + G_u(3)$		1499.8	1502.0	1499
$G_u(1) + H_u(5)$	1	1516.5	1516.5	1514
$H_g(1) + H_g(6)$		1524.0		
$H_g(2) + H_g(5)$	2	1533.5	1532.0	1528
$2H_g(4)$	1	1550.0	1547.0	1544
$H_g(8)$		1577.5[d]	1577.5	1575
$A_g(1) + H_g(5)$		1598.5		
$G_u(3) + H_u(3)$		1620.0	1619.0	
$F_{1g}(3) + H_g(1)$	1	1630.5	1634.0	
$H_g(2) + H_g(6)$		1683.5		1687
$H_g(1) + H_g(7)$	1	1699.5	1693.0[g]	1694
$G_g(1) + H_g(6)$		1737.0	1736.5	
$A_g(2) + H_g(1)$		1743.0		
$A_g(1) + H_g(6)$		1748.5		
$F_{1u}(2) + F_{2u}(4)$	1	1776.8	1776.0	
$F_{1g}(3) + H_g(2)$	4	1790.0	1789.0	
$H_g(3) + H_g(5)$	1	1812.0	1811.0	
$G_g(1) + G_g(5)$	2	1842.0	1841.0	
$H_g(1) + H_g(8)$		1850.5		
$H_g(2) + H_g(7)$	1	1859.0	1857.0	
$H_g(4) + H_g(5)$	2	1876.0	1875.5	
$A_g(2) + H_g(2)$	1	1902.5	1901.0	
$G_g(1) + H_g(7)$	2	1912.5	1913.5	
$A_g(1) + H_g(7)$		1924.0		
$G_u(1) + H_u(7)$	3	1958.5	1959.5	
$H_g(3) + H_g(6)$		1962.0	1959.5	
$A_g(1) + A_g(2)$		1967.5		
$H_g(2) + H_g(8)$	2	2010.0	2006.5	
$H_g(4) + H_g(6)$	1	2026.0	2025.5	
$G_u(3) + H_u(5)$		2041.0	2041.0	
$2F_{2u}(3)$	1	2052.0	2052.5	
$A_g(1) + H_g(8)$	1	2075.0	2070.5	
$F_{2g}(2) + H_g(6)$	1	2116.0	2119.0	
$H_g(3) + H_g(7)$	2	2137.5	2136.0[g]	
$F_{1g}(3) + G_g(3)$	1	2163.5	2167.5	
$A_g(2) + H_g(3)$		2181.0	2180.0	
$H_g(4) + H_g(7)$	2	2201.5	2199.0	
$2H_g(5)$		2202.0	2199.0[g]	
$F_{2u}(3) + F_{2u}(4)$		2227.0	2227.5	
$A_g(2) + H_g(4)$		2245.0	2243.5	
$F_{2u}(5) + H_u(3)$	1	2272.5	2274.0	
$2A_u(1)$		2286.0	2286.0	
$H_g(3) + H_g(8)$		2288.5	2286.0	
$F_{1g}(2) + G_g(5)$	1	2331.5	2331.5	
$F_{1g}(2) + F_{1g}(3)$		2333.0	2331.5	
$H_g(5) + H_g(6)$		2352.0	2350.0[g]	
$H_g(4) + H_g(8)$		2352.5	2350.0	
$F_{2g}(2) + G_g(6)$		2389.5	2393.5	
$F_{2g}(3) + G_g(6)$	1	2438.5	2438.5	
$F_{2g}(4) + H_g(5)$		2461.0	2463.0	
$2H_g(6)$	2	2502.0	2506.0	
$H_g(5) + H_g(7)$	2	2527.5	2527.0[g]	
$F_{1g}(2) + H_g(8)$		2553.0	2551.0	
$A_g(2) + H_g(5)$		2571.0	2570.0	
$F_{1u}(3) + F_{1u}(4)$		2612.1	2611.0	
$F_{1u}(3) + G_u(6)$		2628.9	2629.0	
$G_g(4) + H_g(8)$		2653.0	2653.0	
$H_g(6) + H_g(7)$	1	2676.5	2677.0[g]	
$H_g(5) + H_g(8)$		2678.5	2677.0	
$A_g(2) + H_g(6)$	4	2721.0	2717.0	
$F_{1u}(3) + H_u(7)$		2741.9	2736.0	
$G_g(6) + H_g(6)$		2775.5	2773.5	
$F_{1g}(3) + H_g(7)$	1	2784.0	2782.0	
$H_g(6) + H_g(8)$		2828.5	2823.0	
$2H_g(7)$		2853.0	2850.0[g]	
$A_g(2) + H_g(7)$		2896.5	2896.5	
$2A_g(2)$		2940.0	2940.5[g]	
$H_g(7) + H_g(8)$	1	3004.0	3002.0[g]	
$A_g(2) + H_g(8)$	1	3047.5	3046.0	
$2H_u(7)$		3118.0	3118.0	
$F_{2u}(5) + H_u(7)$		3135.5	3134.0	
$2H_g(8)$	1	3155.0	3152.0[g]	
			3267.0	
			3282.0	
			3325.0	
			3385.0	

[a] All overtone and combination modes of first-order A_g and H_g modes are listed. Selected combinations involving silent modes are also listed. Most of these modes were shifted from the values quoted in Ref. 5 to better fit the observed second-order spectrum. For the silent modes, the values in cm^{-1} are F_{1g}, 502.0, 975.5, 1357.5; F_{2g}, 566.5, 865.0, 914.0, 1360.0; G_g, 486.0, 621.0, 806.0, 1075.5, 1356.0, 1524.5; A_u, 1143.0; F_{1u}, 526.5, 575.8, 1182.9, 1429.2; F_{2u}, 355.5, 680.0, 1026.0, 1201.5, 1576.5; G_u, 399.5, 760.0, 924.0, 970.0, 1310.0, 1446.0; H_u, 342.5, 563.0, 696.0, 801.0, 1117.0, 1385.0, 1559.0.

[b] Number of other possible second-order combination modes within ±3 cm^{-1} of the experimental line.

[c] From the work of van Loosdrecht *et al.* (Ref. 10).

[d] Mode frequencies used as input parameters for predicting the overtone and combination modes.

[e] Forbidden Raman mode possibly activated by isotopic substitution ($^{13}C^{12}C_{59}$).

[f] A silent mode listed in (a) is also a possible identification for this mode.

[g] Also observed and identified similarly by Denisov *et al.* (Ref. 11).

Below $\sim$1700 cm^{-1} a very similar spectrum to that shown in Fig. 1 has been reported by van Loosdrecht *et al.*[10] at $T = 40$ K for single-crystal C_{60}. These frequencies at 40 K are also given in Table I and are in good agreement with the present work. However, in contrast to the present work, all the features below $\sim$1700 cm^{-1} in Ref. 10 are identified with crystal-field-induced splittings of first-order-allowed (H_g) modes or crystal-field-activated silent modes ($G_g, F_{1g}, F_{2u}, F_{2g}$) or activated IR modes (F_{1u}).[10]

We now discuss the region in Fig. 1 above the highest first-order Raman mode $H_g(8) = 1577.5$ cm^{-1}. In the absence of impurities, spectral features in this region must be assigned to second- and higher-order scattering processes. In fact, the lower bound for both the second- and third-order scattering in a sum process is in the range of the first-order scattering [$2H_g(1) = 546.0$ cm^{-1} and $3H_g(1) = 819.0$ cm^{-1}]. As before, it is seen in Fig. 1 that most of the structure above the $H_g(8)$ mode in the spectrum at 20 K survives at very high temperature (523 K), albeit broadened thermally. The vertical lines in the figure are plotted at the positions of all the sum combinations $\omega_1(\Gamma_1)+\omega_2(\Gamma_2)$, where Γ_1 and Γ_2 have either A_g or H_g symmetry. Thus the vertical lines correspond to combination modes involving only modes which are first-order allowed. However, several tentative assignments involving a "silent" mode partner in $(\omega_1 + \omega_2)$ scattering are also given in Table I. At high T, mode anharmonicity effects appear to significantly shift some of the higher-order lines relative to their positions at 20 K.

In summary, we make tentative assignments in Table I to all the features observed in the 20-K Raman spectrum. As can be seen from Table I, several of the observed lines are explained by combination mode scattering involving only silent modes. Since the silent mode frequencies for C_{60} are known to less precision than the A_g and H_g modes, this work serves to refine almost all of the silent modes in terms of their mode frequencies and symmetry assignments. All but two [$H_u(4) = 801.0$ cm^{-1} and $H_u(6) = 1385.0$ cm^{-1}] have been determined from the fit to the higher-order Raman spectrum. These two modes are taken from Ref. 5. In the fitting procedure, the first-order Raman and infrared-active modes were considered as fixed by previous experiments, and the even-parity silent modes were determined by identification of higher-order lines consisting of one optically active mode and one silent mode. The remaining odd-parity silent modes were then determined by fits to well-resolved higher-order features, using the frequency assignments in Ref. 5 as a first-order approximation. Below $\sim$1000 cm^{-1} several lines superscripted by "e" in the identification column of Table I are assigned to isotopically activated first-order modes. Further work on isotopically pure $^{12}C_{60}$ will be necessary to clarify the identification of these lines.

Note added in proof. Using transmission FTIR spectroscopy on 4-μm-thick C_{60} films grown on KBr substrates, we have recently observed numerous ($\sim$ 100) sharp, infrared-active lines in addition to the four strong, first-order $F_{1\mu}$ symmetry modes. Similar to the work reported here, most of these lines can be assigned to second-order, intramolecular combination modes, although several of the lines below $\sim$ 1000 cm^{-1} appear to be first-order (IR-forbidden) modes activated by isotopic substitution.

J.M.H. and P.C.E. were supported by the University of Kentucky Center for Applied Energy Research and the NSF Grant No. EHR-91-08764. M.S.D. and G.D. acknowledge support from NSF Grant No. DMR-92-01878.

[1] P. C. Eklund *et al.*, J. Phys. Chem. Solids **53**, 1391 (1992).
[2] P. Zhou *et al.* (unpublished).
[3] Y. Wang *et al.* (unpublished).
[4] A. M. Rao *et al.*, Science **259**, 955 (1993).
[5] R. A. Jishi, R. M. Mirie, and M. S. Dresselhaus, Phys. Rev. B **45**, 13 685 (1992).
[6] P. C. Painter and J. L. Koenig, Spectrochim. Acta Part A **33**, 1003 (1977).
[7] G. Dresselhaus, M. S. Dresselhaus, and P. C. Eklund, Phys. Rev. B **45**, 6923 (1992).
[8] P. A. Heiney *et al.*, Phys. Rev. Lett. **66**, 2911 (1991); see also Comment by R. Sachidanandam and A. B. Harris, *ibid.* **67**, 1467 (1991).
[9] W. I. F. David *et al.*, Europhys. Lett. **18**, 219 (1992); **18**, 735 (1992).
[10] P. H. M. van Loosdrecht, P. J. M. van Bentum, M. A. Verheijen, and G. Meijer, Chem. Phys. Lett. **198**, 587 (1992).
[11] V. N. Denisov *et al.*, Zh. Eksp. Teor. Fiz. **102**, 300 (1992) [Sov. Phys. JETP **75**, 158 (1992)].